applied sciences

MDPI

Article

A Novel Criticality Analysis Method for Assessing Obesity Treatment Efficacy

Shadi Eltanani [1,*], Tjeerd V. olde Scheper [1], Mireya Muñoz-Balbontin [1], Arantza Aldea [1], Jo Cossington [2], Sophie Lawrie [2], Salvador Villalpando-Carrion [3], Maria Jose Adame [3], Daniela Felgueres [3], Clare Martin [1] and Helen Dawes [4]

[1] School of Engineering, Computing and Mathematics, Faculty of Technology, Design and Environment, Oxford Brookes University, Wheatley Campus, Wheatley, Oxford OX33 1HX, UK; tvolde-scheper@brookes.ac.uk (T.V.o.S.); aaldea@brookes.ac.uk (A.A.); cemartin@brookes.ac.uk (C.M.)
[2] Centre for Movement and Occupational Rehabilitation Sciences (MOReS), Oxford Brookes University, Oxford OX3 0BP, UK; jcossington@brookes.ac.uk (J.C.); sophielawrie@hotmail.co.uk (S.L.)
[3] Hospital Infantil de Mexico Federico Gomez, Mexico City 06720, Mexico; villalpandoca@himfg.edu.mx (S.V.-C.); mariajose@adame.com.mx (M.J.A.); danielafelgueresn@gmail.com (D.F.)
[4] National Institute for Health and Care Research (NIHR) Exeter Biomedical Research Centre, University of Exeter, St Luke's Campus, Exeter EX1 2LU, UK; h.dawes@exeter.ac.uk
* Correspondence: seltanani@brookes.ac.uk

Abstract: Human gait is a significant indicator of overall health and well-being due to its dependence on metabolic requirements. Abnormalities in gait can indicate the presence of metabolic dysfunction, such as diabetes or obesity. However, detecting these can be challenging using classical methods, which often involve subjective clinical assessments or invasive procedures. In this work, a novel methodology known as Criticality Analysis (CA) was applied to the monitoring of the gait of teenagers with varying amounts of metabolic stress who are taking part in an clinical intervention to increase their activity and reduce overall weight. The CA approach analysed gait using inertial measurement units (IMU) by mapping the dynamic gait pattern into a nonlinear representation space. The resulting dynamic paths were then classified using a Support Vector Machine (SVM) algorithm, which is well-suited for this task due to its ability to handle nonlinear and dynamic data. The combination of the CA approach and the SVM algorithm demonstrated high accuracy and non-invasive detection of metabolic stress. It resulted in an average accuracy within the range of 78.2% to 90%. Additionally, at the group level, it was observed to improve fitness and health during the period of the intervention. Therefore, this methodology showed a great potential to be a valuable tool for healthcare professionals in detecting and monitoring metabolic stress, as well as other associated disorders.

Keywords: human gait; criticality analysis; support vector machine

Citation: Eltanani, S.; olde Scheper, T.V.; Muñoz-Balbontin, M.; Aldea, A.; Cossington, J.; Lawrie, S.; Villalpando-Carrion, S.; Adame, M.J.; Felgueres, D; Martin, C.; et al. A Novel Criticality Analysis Method for Assessing Obesity Treatment Efficacy. *Appl. Sci.* **2023**, *13*, 13225. https://doi.org/10.3390/app132413225

Academic Editors: Arkady Voloshin, Chien-Hung Yeh, Wenbin Shi, Xiaojuan Ban, Men-Tzung Lo and Shenghong He

Received: 18 August 2023
Revised: 2 November 2023
Accepted: 7 December 2023
Published: 13 December 2023

1. Introduction

Human gait, the intricate orchestration of biomechanical movements during ambulation, stands as a pivotal aspect of human motor function with far-reaching implications for an individual's health and overall wellbeing [1–3]. This intricate phenomenon, however, is not a static entity. It is subject to perturbations stemming from a diverse array of factors, encompassing injuries, diseases, disorders, and external conditions, thereby engendering deviations from established norms and the emergence of irregular or aberrant gait patterns [4–6].

The traditional methodologies employed in gait analysis, predominantly reliant upon observational techniques, possess inherent limitations marked by subjectivity and inter-observer variability [7]. These methodologies, furthermore, confront difficulties in adequately encapsulating the nuanced, multifaceted, and quantitative attributes inherent

in gait, particularly when confronted with intricate patterns stemming from underlying pathologies [8].

In the contemporary landscape of medical diagnostics, artificial intelligence (AI) has emerged as a promising frontier, bearing the capacity to substantially enhance gait analysis and expedite the detection of gait-related disorders [9,10]. Its proficiency in the processing of extensive datasets, identification of latent patterns, and facilitation of early diagnoses offers substantial promise [11]. Nonetheless, AI grapples with intricate challenges in the realm of gait analysis, stemming from the dynamic nature of gait itself and the intricate interplay of a multitude of contributory factors [11].

In response to these exigencies, this paper introduces Criticality Analysis (CA) as an innovative and robust AI tool primed for precise identification of abnormal or irregular gait patterns, thereby indicating the presence of latent disorders or ailments. Beyond its diagnostic prowess, CA serves as a dynamic tool for the continuous monitoring of disorder progression and the systematic tracking of treatment efficacy over temporal trajectories. This innovative paradigm promises to empower medical practitioners in their clinical decision making in relation to gait-related disorders, ultimately effecting substantial enhancements in patient outcomes and the broader landscape of healthcare.

The paper is structured as follows: Section 2 outlines a methodology employing mathematical models to assess critical aspects of human gait, emphasising the integration of mathematical modeling and criticality analysis in the context of gait study. In Section 3, the methodology applied to the Criticality Analysis of Diabetic Gait in Children (CARDIGAN) dataset is detailed, covering data collection, feature extraction, criticality analysis data representation, and spatiotemporal analysis. Section 4 explores the experimental results of the CARDIGAN dataset, including the analysis of Receiver Operating Characteristic (ROC) Curves, the calculation of Area Under the Curve (AUC), and the determination of the decision boundary of the support vector method. Section 5 provides a concise summary of the overarching results, while Section 6 concludes by highlighting the key findings of the research.

2. Mathematical Model-Driven Criticality Analysis for Human Gait Assessment

The complexities of human locomotion have long intrigued researchers who strive to decode the dynamic, self-organised patterns underlying gait. With each step, the intricately choreographed motions blur the boundary between conscious control and automated processes. Gait is governed by nonlinear phenomena, including emergent oscillations, traveling waves, and spiraling coordination, which evolve across spatiotemporal scales. To decipher the chaotic fluctuations disrupting normal walking, mathematical models become indispensable, capturing nuanced biomechanics within the motor control system [12]. Particularly intriguing is the analysis of disruptions propelling gait into criticality, marked by surges in kinetic energy and resulting in near power-law and exponential dynamics. The human locomotive system, while captivating, lacks comprehensive models characterising its dynamics across both temporal and spatial dimensions. Simplified models often cannot fully capture the complex control mechanisms translating network behavior into stable, coordinated movement patterns across space. Therefore, developing sophisticated models is crucial for decoding the inherent complexities of human gait and locomotion.

In this paper, we employ a nonlinear biochemical enzyme control model to conduct a comprehensive analysis of human gait dynamics, shedding new light on the intricate biomechanical processes underlying locomotion [13]. In this paper, the investigation is centered on elucidating the specific role of biochemical reactions in shaping gait patterns. This meticulous exploration of biochemical intricacies allows for discerning their profound influence on the overall coordination and characteristics of human gait. This modeling approach gains particular relevance when examining scenarios where particular biochemical pathways are suspected to be pivotal factors contributing to gait abnormalities or adaptations, as often observed in various pathological conditions.

The model utilises a control mechanism to stabilise external perturbations to the motor system by precisely calibrating the quantity of enzyme in relation to the concentration of one of the variables, f. The model also represents the control process of two enzymes that govern the formation of the extracellular matrix, m, from soluble filaments, f. The proteinase, p, deconstructs the matrix into filaments, while transglutaminase, g, reassembles the filaments into the matrix. The extracellular matrix, m, is continually generated by adjacent cells, r_{im}, at a constant rate, with each protein undergoing catalytic processes proportional to p. The bifurcation parameter, r_{im}, acts as an external turbulent input to the control model. The dynamics governing the rate of enzyme production, specifically enzymes p and g, are influenced by the Rate Control of Chaos (RCC). This approach employs a series of nonlinear rate equations, as illustrated in Equations (4)–(7), to describe the temporal evolution of system variables. A key control term in these rate equations contains variable f, which has a strong nonlinear influence on the dynamics. The RCC confines this control term using a rate control function, as depicted in Equation (1), that restricts its divergence rate, thereby stabilising the overall system behavior. The adjustable parameters in the rate control function allow tuning the intensity of control applied to the chaotic dynamics. Meanwhile, the criticality analysis involves examining the phase space representation of outputs f and m, which correspond to concentrations of soluble filaments and extracellular matrix, respectively. The phase space plot with f on the x-axis and m on the y-axis illustrates the time-dependent evolution of nonlinear dynamics. As parameters are varied, the system exhibits complex phenomena, including bistability, limit cycles, spiralling trajectories, and chaos, particularly near critical transition points. Analysing the geometric patterns within the phase portrait provides valuable insights into the mechanisms underpinning self-organised criticality. Characteristics such as the number and stability of fixed points, oscillations, excitability, and susceptibility to perturbations can be deduced from phase space topology. Additionally, the fractal-like features within the phase portrait unveil the self-similar, scale-invariant nature of critical fluctuations. Moreover, this representation facilitates the quantification of nonlinear correlations that capture the intricacies of coupled dynamics. Therefore, phase space-based criticality analysis unveils the system's rich nonlinear behavior, phase transitions, and emergent complexity resulting from self-organised criticality.

$$q_f = \frac{f}{f + \mu_f}, \tag{1}$$

$$\sigma_p(q_f) = f_p e^{(x_p q_f)}, \tag{2}$$

$$\sigma_g(q_f) = f_g e^{(x_g q_f)}, \tag{3}$$

$$\frac{dm}{dt} = k_g \frac{fg}{K_G + f} - \frac{mp}{1+m} + r_{im}, \tag{4}$$

$$\frac{df}{dt} = -k_g \frac{fg}{K_G + f} + \frac{mp}{1+m} - \frac{fp}{1+f}, \tag{5}$$

$$\frac{dp}{dt} = \sigma_p(q_f)\gamma \frac{f^n}{K_R^n + f^n} - k_a p^2, \tag{6}$$

$$\frac{dg}{dt} = \sigma_g(q_f)\beta \frac{f^l}{K_S^l + f^l} - k_{deg} \frac{gp}{K_{deg} + g}. \tag{7}$$

Mathematically speaking, the CA model has several parameters, including $\gamma = 0.026$, $\beta = 0.00075$, $K_R = 4.5$, $K_S = 1$, $K_G = 0.1$, $K_{deg} = 1.1$, $k_g = k_{deg} = 0.05$, and $k_a = \frac{k_{deg}}{K_{deg}} = 0.0455$. Hill numbers n and l are also set to four. Bifurcation parameter r_{im} exhibits a wide range of dynamic behaviors, including stable periodic cycles, bistability, and chaos. This parameter remains constant for all oscillators within the chaotic domain. Additionally, an external input is applied as a perturbation to the r_{im} parameter as described in Equation (8). This parameter links different oscillators together by using a relative scale contribution from all other oscillators. RCC control parameters presented in Equations (1)–(3) ($f_p = f_g = 1$, $x_p = x_g = -1$, and $\mu_f = 2$) are kept constant throughout the experiment simulations in this paper, but can have different values that allow the local oscillator possibility to change its oscillatory orbits.

$$r_{im}{}^{i} = \sum_{j=1, j\neq i}^{n} w_j m_j + \varepsilon. \tag{8}$$

The connectivity strength between various oscillators, represented by w_j, can range from 0.00011, 0.00012, to 0.00025. External perturbations, represented by ε, are uniformly distributed according to a Gaussian distribution and scaled within the domain of $[-1, 1]$. These perturbations are observed over a range of evolution steps to explore the varying oscillatory cycles they produce. In this paper, a connectivity strength of $w_j = 0.0002$ was selected from the chaotic domain of the underlying oscillators to assess its effect on the dynamics while maintaining overall stability.

The network of nonlinear models in this paper consists of 16 oscillators, each of which can adjust their local dynamics to adapt to external perturbations from their neighboring oscillators. The simulation of the entire model was carried out using EuNeurone software (v2.3, 2013) and the Fehlberg-RK method as a fixed step integration for Ordinary Differential equations (ODEs). The total unweighted dynamics, represented by M and F in Equations (9) and (10), were measured as the net sum of the individual oscillators, allowing for observation by a remote observer who would otherwise be unable to detect the individual oscillators.

$$M = \sum_{i=1}^{n} m_i, \tag{9}$$

$$F = \sum_{i=1}^{n} f_i. \tag{10}$$

The CA method described in this paper has previously been applied in research, leveraging its capabilities to generate dynamic and scale-free nonlinear data representations, which in turn facilitate the precise detection of disturbances associated with human gait [14]. Subsequently, CA combined these encoded representations with the SVM algorithm, enhancing superior detection accuracy. This synergy surpasses traditional methods that lack the CA approach in terms of performance and robustness. Hence, this innovative CA approach allows for the generation of nonlinear data representations that are well suited for training conventional classifiers [15].

3. Methodology

The proposed CA method for classifying human gait disorders includes a framework consisting of several key components, including data collection, data processing, feature extraction, and the use of the SVM technique. This methodology is illustrated in Figure 1.

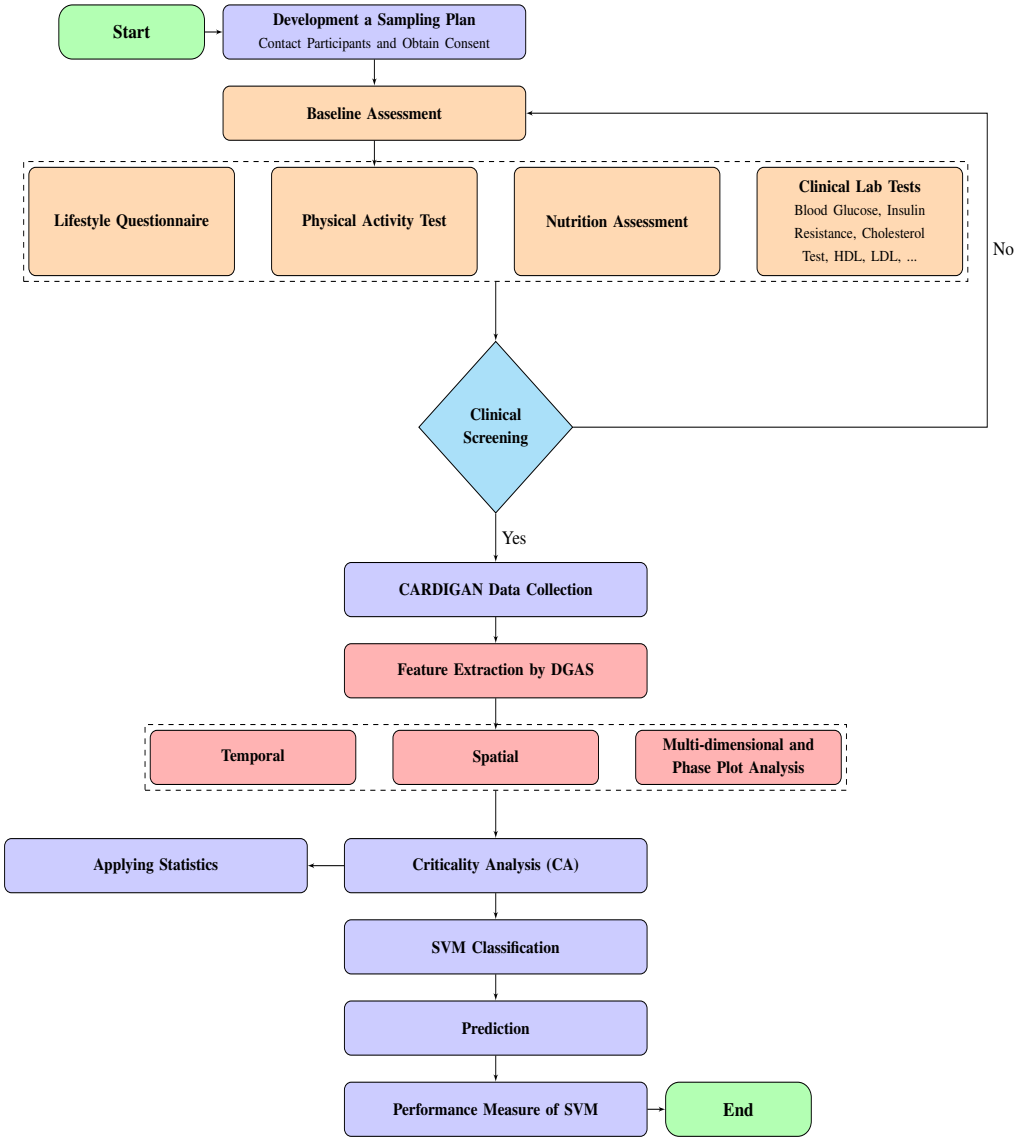

Figure 1. The flowchart of the proposed CARDIGAN methodology is presented.

3.1. Data Collection

The study assembled a heterogeneous cohort of 50 adolescent subjects, comprising individuals diagnosed with obesity, those with diabetes, and a cohort of healthy controls, all of whom were thoroughly recruited from Mexico Children's Hospital. Among the healthy control group, 19 were males, and there was one female participant, with ages ranging from 10 to 15 years, weights spanning from 40 to 83 kg, heights from 133 to 172.9 cm, and BMIs from 21.16 to 34. The participants with obesity included 16 males and 4 females, aged between 10 and 17 years, with weights ranging from 36 to 106.4 kg, heights spanning from 129 to 179 cm, and BMIs from 17.64 to 35.5. Meanwhile, diabetic participants consisted of 10 females aged 12 to 13 years, with weights ranging from 74.5 to 76.2 kg, heights from 159 to 159.7 cm, and BMIs from 29.5 to 30.4. It is crucial to underscore that due to an inadequate volume of available diabetic data points, the analysis was restricted to data from 20 healthy controls and 20 participants diagnosed with obesity, ensuring the robustness of the findings while acknowledging data limitations. The participants underwent a 6-week intervention program aimed at improving fitness and reducing weight. Gait analysis was conducted at baseline, immediately after the intervention, and at 3- and 6-month follow-ups. Gait analysis involved participants walking back and forth over a 30 m track for 6 min while

wearing an inertial measurement unit sensor on their lower back. The gait data were anonymised, and approval was obtained before analysis.

Assessment was based on the use of an inertial measurement movement sensor (IMU), placed on the fourth lumbar vertebra located on the top left of the anatomical position of the lumber spine, known as the body Centre of Mass (CoM). The sensor was designed to be incredibly flexible, providing for mobility in many different planes including flexion, extension, side bending, and rotation. Gait analysis was conducted for participants using a standardised 6 m test, wherein an IMU was attached to the lower back to capture triaxial accelerometer and gyroscope data at a frequency of 100 Hz. For individuals with DPN (Diabetic Peripheral Neuropathy), the assessment took place at OCDEM (Oxford Centre for Diabetes, Endocrinology, and Metabolism) in a dedicated obstacle-free corridor. The methodology employed for deriving gait parameters has been comprehensively described in previous studies. The spatiotemporal parameters obtained from the 6 min walking test encompassed step time (measured in milliseconds), cadence (expressed in steps per minute), stride length (in meters), and walking speed (in meters per second). Furthermore, gait control parameters, which encompass measures of dynamic stability and gait variability, were evaluated utilising various instruments such as accelerometers, force plates, or motion capture technology. These assessments aimed to quantify fluctuations in temporal aspects (e.g., stride time), spatial aspects (e.g., step length), and comprehensive whole-body kinematics (e.g., segment angles). The parameters assessed included Beta (expressed in degrees), SDa (measured in arbitrary units), SDb (also in arbitrary units), ratio (in a dimensionless unit), and walk ratio (in millimeters per steps per minute). These parameters have been identified as indicators of neuro motor control [16,17]. The dynamics of their walking activity were monitored using the Polar Team tracking system [18].

3.2. Feature Extraction Method for Analysing Gait Data

The CARDIGAN dataset, which was collected utilising a 3-dimensional accelerometer, gyroscope, and magnetometer IMU sensor, was analysed utilising DataGait Analysis Software (DGAS) (v11.1, 2019). Developed as a standalone software analysis package by the Movement Science Group at Oxford Brookes University using LabVIEW2011 (National Instruments, Ireland), DGAS employs quaternion rotation matrices and double integration to transpose the accelerations frame of the z-axis from the object to the global system, thereby allowing for the measurement of translatory vertical CoM accelerations during walking and the achievement of a relative change in position. As referenced in [18], upward CoM measurements determine the global quality of human gait parameters. DGAS extracts critical features of individuals' gait for the purpose of classification. In this context, it becomes feasible to differentiate between biologically distinct masculine and feminine gait patterns, taking into account not only the spatiotemporal parameters that capture gait dynamics at specific time points but also the potential impact of their respective body shapes or dimensions on these distinctions. In gait analysis, a multitude of parameters are employed to comprehensively understand the complexities of human locomotion. Temporal parameters encompass fundamental measurements such as Step Time, which quantifies the duration from the initial contact of one foot to the subsequent contact of the opposite foot, and Stride Time, which denotes the time interval between successive initial contacts of the same foot. Cadence adds another layer of insight, representing the number of steps taken per unit of time. Meanwhile, spatial parameters offer dimensions to gait assessment; Step Length measures the distance between successive initial contacts of the same foot, and Stride Length extends this to cover the span from one foot's initial contact to the following foot's contact. The rate of position change during gait, known as Velocity, is calculated by the ratio of stride length to stride time. In addition, multi-dimensional parameters introduce complexity: Duty Factor gauges the percentage of the gait cycle during which each foot remains on the ground, while the Froude Number serves as a dimensionless speed parameter reflecting the interplay of centripetal and gravitational forces during walking. Finally, the Walk Ratio denotes the relationship between cadence

and mean step length, offering insights into the neuromotor control of gait. Within the realm of Phase Plot Analysis, distinctive parameters emerge: Beta Angle, a measure of stability, is the angle of the primary gait phase plot axis relative to the vertical axis; SDa and SDb represent standard deviations describing the distribution of phase plot points, with SDa reflecting stability and SDb pertaining to rhythm; and Ratio (SDa/SDb) serves as a relative rhythm stability indicator. The raw data from the accelerometer are processed using DGAS software, which is founded on the inverted pendulum approach. This conversion results in 17 parameters that are used to assess the physical characteristics of each individual. These 17 gait features serve as inputs for perturbing the criticality analysis model, as represented by Equations (4) and (7), respectively. Table 1 displays the list of the 17 gait parameters.

Table 1. Extracted Gait Features.

Gait Parameter	Measurement	Unit
Temporal	Step Time	(ms)
	Step Time (Left)	(ms)
	Step Time (Right)	(ms)
	Stride Time	(ms)
	Cadence	(steps/min)
Spatial	Step Length (Left)	(m)
	Step Length (Right)	(m)
	Stride Length	(m)
	Velocity	(m/s)
Multi-dimensional	Duty Factor Double Stance	(%)
	Duty Factor Single Stance	(%)
	Froude Number	(au)
	Walk Ratio	(mm/steps/min)
Phase Plot Analysis	Beta Angle	(Degree (°))
	SDa	(au)
	SDb	(au)
	Ratio = SDa/SDb	(Dimensionless)

3.3. Gait Data Representation and Spatiotemporal Analysis Using Criticality Analysis

Criticality Analysis is a method used to represent complex multivariate data patterns in a simplified form, typically in the form of a phase plot portrait or manifold. This method involves analysing the data in multiple dimensions and identifying patterns or structures that are most critical to understanding the underlying dynamics of the system. The extracted features by DGAS were used as perturbation inputs to the CA model represented by Equations (4) and (7), respectively. This aided in gaining a deeper understanding of the underlying mechanisms and dynamics of the system under study. The visual representations of gait regulation and coordination between spatial and temporal domains are depicted in Figures 2–7 through phase plot orbits. Well-regulated gait was characterised by smooth and narrow orbits, whereas dysfunctional gait control was evident in irregular and variable orbits. These phase plots served as a means to distinguish between healthy and pathological gaits by evaluating the dynamics of spatiotemporal coordination. These phase plots demonstrated clear differences between the gait patterns of the healthy control and obesity groups over the 6-week period. Specifically, in the healthy control group, the phase plots exhibited a consistent pattern characterised by smooth and regular oscillations with steady amplitudes and frequencies. These findings were indicative of a well-maintained, rhythmic gait pattern that demonstrated excellent coordination and balance. Notably, the orbits in this group remained relatively narrow, which underscored the efficiency of their biomechanics and the minimal occurrence of side-to-side body motion. In contrast, the obesity group displayed phase plots that deviated from the healthy control group's pattern. These plots appeared more irregular and distorted, with variable amplitudes and wider orbits, suggesting a compromised sense of balance and increased lateral swaying

during gait. Furthermore, these phase plots exhibited more abrupt changes in direction, indicating the need for sudden adjustments to maintain stability. These observations were reflective of a slower and more effortful gait, likely resulting from the additional weight burdening the joints and muscles in individuals with obesity. Moreover, both groups exhibited a common trend of declining gait consistency over the 6-week observation period, potentially attributable to the onset of fatigue effects. The healthy control group, despite its initial robust gait pattern, displayed a gradual decrease in consistency, reflecting the possibility of accumulating fatigue from repeated gait assessments. The obesity group, already experiencing challenges in maintaining gait regularity, showed a similar decline in consistency, accentuating the toll that prolonged observation sessions might take on their gait patterns. This convergence in declining gait consistency underscores the importance of considering potential fatigue factors in the interpretation of gait analysis results across different population groups.

Examining the gait patterns across the 6-week period, in Figure 2 (Week 1), the healthy group displayed a tight circular cluster, indicating consistent gait cycles. In contrast, the obesity group showed more elongated, scattered orbits, reflecting a higher degree of variability in gait. As we progressed to data depicted in Figure 3 (Week 2), the healthy group continued to maintain a tight cluster, while the obesity group's orbits, though still dispersed, appeared somewhat more rounded, suggesting some improvement in gait coordination compared to that of Week 1. Figure 4 (Week 3) portrayed the healthy group with a very tight cluster, indicative of highly consistent gait, while the obesity group exhibited more elongated orbits with flatter tops, indicating instability in their gait pattern. In Figure 5 (Week 4), the healthy control cluster became somewhat looser, possibly due to accumulating fatigue. The obesity group's orbits remained uneven but showed a slightly improved level of coordination compared to Week 3. Figure 6 (Week 5) demonstrates the healthy control group's cluster becoming more dispersed, reflecting increasing gait variability. On the other hand, the obesity group's plots were highly scattered with jagged trajectories, suggesting a worsening of gait control. Finally, in Figure 7 (Week 6), both groups display more dispersed orbits than in previous weeks, indicating the potential impact of fatigue on gait consistency in both groups. The obesity group's orbits appeared slightly more rounded than in Week 5, hinting at some recovery in coordination, although the overall trend indicated challenges in maintaining consistent gait patterns.

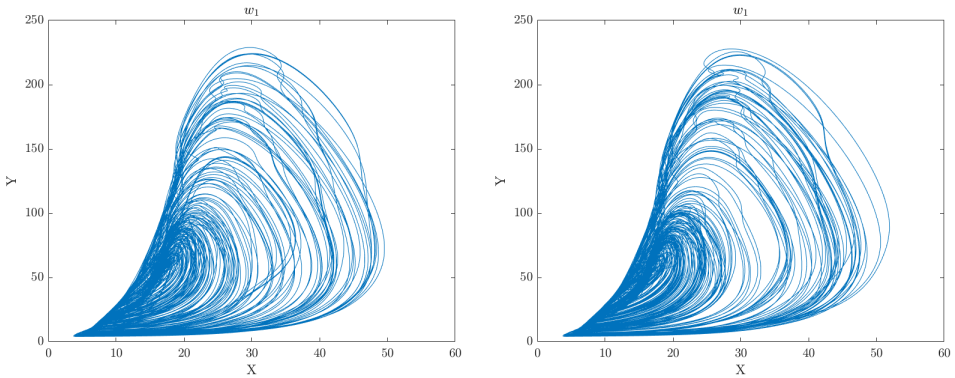

Figure 2. Comparison of phase space plots of walk patterns for healthy control and obesity groups in the clinical gait experiment conducted in w_1 is presented. Healthy control walk patterns are shown on the left while obesity walk patterns are shown on the right.

In this paper, we utilised a kernel SVM classifier to distinguish between the obesity and healthy groups based on phase plot data. The choice of kernel SVM is particularly well suited for this analysis due to the inherently nonlinear and complex nature of the data. Phase plot data, representing dynamic patterns of physiological processes, often exhibit intricate and nonlinear relationships. Traditional linear classifiers may struggle to capture the patterns present in such data. However, the kernel SVM is designed to address this challenge by mapping the data into a higher-dimensional space, where complex patterns

become more separable. It leverages a diverse set of kernel functions, including radial basis function (RBF), to effectively transform the data into a format where it can distinguish between the obese and healthy groups. This approach enables the identification of hidden patterns, making it an ideal choice for this study, and ensures that the classification approach is capable of handling the inherent nonlinearity in the phase plot data, facilitating the reliable and accurate differentiation of the two groups. Figures 16–18 demonstrate the decision boundary generated by kernel SVM, highlighting its effectiveness in distinguishing between obese and healthy control groups using phase plot data.

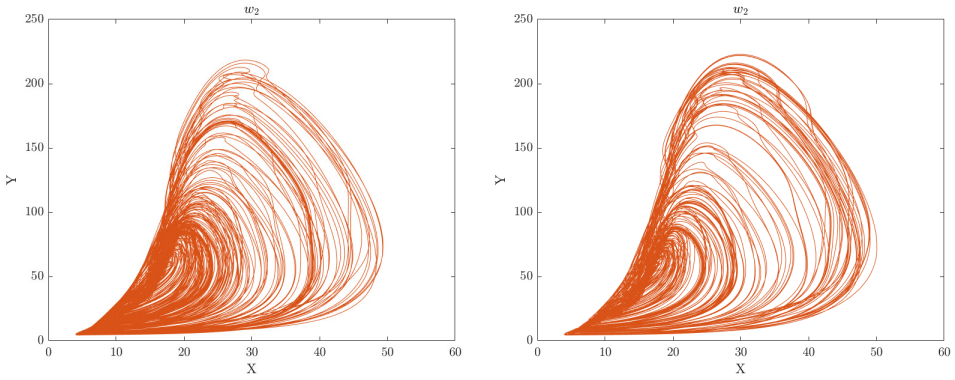

Figure 3. Comparison of phase space plots of walk patterns for healthy control and obesity groups in the clinical gait experiment conducted in w_2 is presented. Healthy control walk patterns are shown on the left while obesity walk patterns are shown on the right.

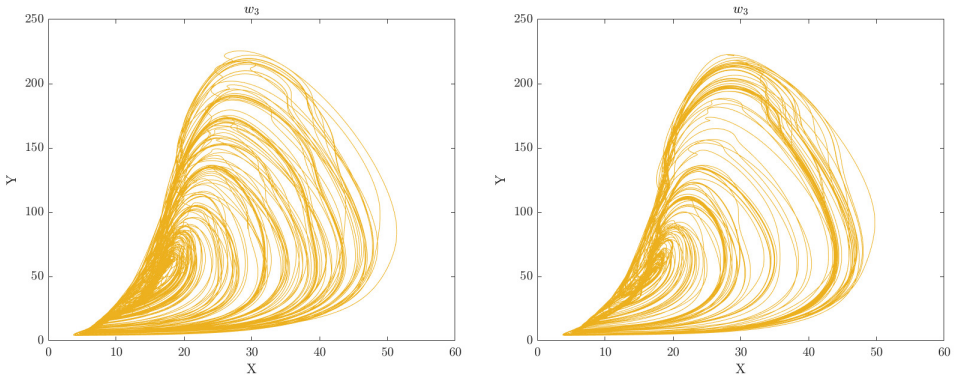

Figure 4. Comparison of phase space plots of walk patterns for healthy control and obesity groups in the clinical gait experiment conducted in w_3 is presented. Healthy control walk patterns are shown on the left while obesity walk patterns are shown on the right.

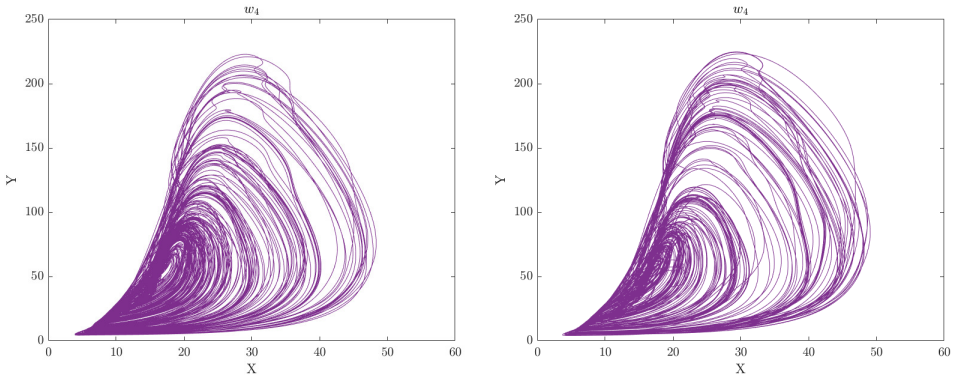

Figure 5. Comparison of phase space plots of walk patterns for healthy control and obesity groups in the clinical gait experiment conducted in w_4 is presented. Healthy control walk patterns are shown on the left while obesity walk patterns are shown on the right.

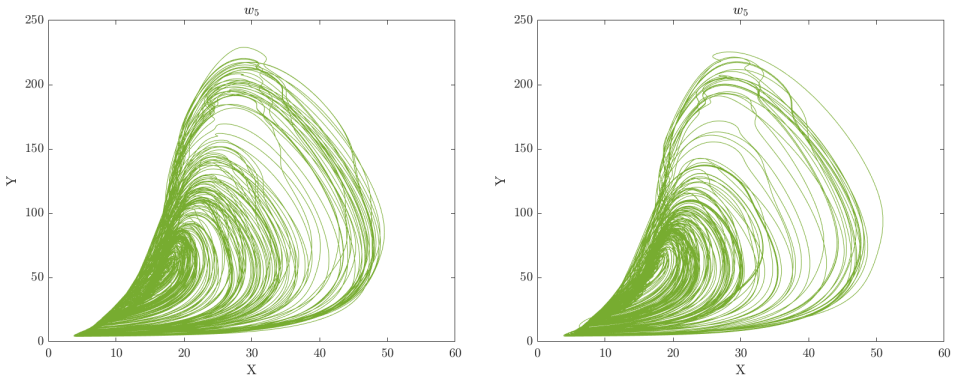

Figure 6. Comparison of phase space plots of walk patterns for healthy control and obesity groups in the clinical gait experiment conducted in w_5 is presented. Healthy control walk patterns are shown on the left while obesity walk patterns are shown on the right.

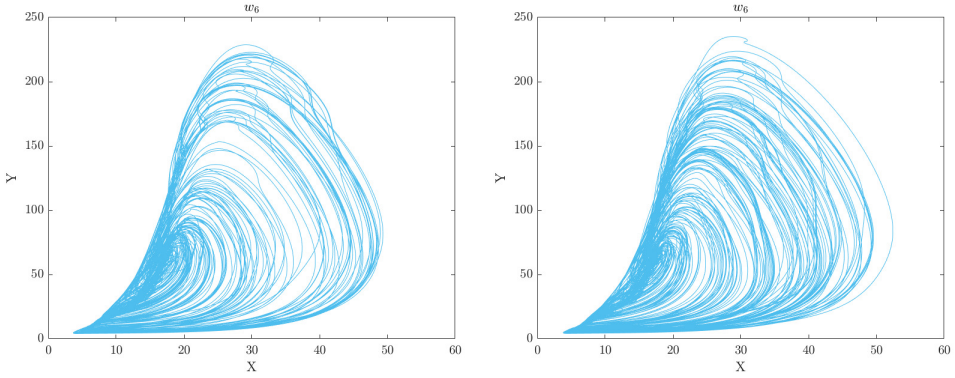

Figure 7. Comparison of phase space plots of walk patterns for healthy control and obesity groups in the clinical gait experiment conducted in w_6 is presented. Healthy control walk patterns are shown on the left while obesity walk patterns are shown on the right.

Figures 8 and 9 serve as invaluable tools for assessing the dynamic nature of gait progression throughout the 6-week study period. These graphical representations offered a comprehensive view of the data by plotting the peak values extracted from each phase plot orbit as discrete data points for every week. Consequently, these visualisations effectively generated trajectories that unveiled nuanced alterations in gait patterns over time. Fundamentally, each data point within these trajectories captured the maximum step length achieved during a specific gait cycle, encapsulating the essence of gait performance. By plotting these peak values across the 6-week observation window, an intuitive visual perspective emerged on how maximal step length evolved across multiple visits. Furthermore, these peak values functioned as numerical metrics that concisely represented the range of variability, which is an informative measure quantifying the degree of variation in maximal step length from one week to the next. To provide a rigorous statistical summary of this variation over time, standard deviation (SD) of the peak values for each participant was calculated. This SD became a pivotal indicator, with a higher value signifying a greater degree of inconsistency in the maximal step length achieved across different weeks. Consequently, comparing SD values before and after the intervention yielded a quantitative assessment of whether gait improved (resulting in a lower SD) or deteriorated (resulting in a higher SD). This analytical approach enabled the precise quantification of the impact of the intervention on gait stability and consistency, offering valuable insights into the effectiveness of the intervention. In Figure 8, which pertains to healthy controls, the majority of trajectories exhibited minimal fluctuation, remaining relatively level throughout the study duration. This observation signified consistent gait patterns from week to week, characterised by limited variation in peak values. Conversely, in Figure 9, representing the obesity group, the trajectories displayed greater irregularity, featuring discernible peaks and troughs across

the weeks. This pattern indicated increased instability in gait parameters, with significant variations in the peak values across the different visits. As an illustrative example, participant P14 was considered. In Figure 8, P14's trajectory remained consistently around 0.55, demonstrating a steady gait with little variation over time. However, in Figure 9, P14's trajectory exhibited a drop from approximately 0.7 to 0.4 by Week 3 before subsequently rebounding. This trajectory pattern suggested that P14's gait became more irregular during the course of the study but later exhibited improvement. Complementing these trajectories, the standard deviation bars visually represented the extent of variability across the 6 weeks. In Figure 8, P14's standard deviation bars were notably small, confirming minimal fluctuation and consistent gait during the pre-intervention period. In contrast, Figure 9 portrayed larger standard deviation bars, indicating increased inconsistency in gait patterns when P14 was in an obese state. Overall, these quantitative comparisons between Figures 8 and 9 provided valuable insights into the differences in gait stability and variability between individuals with obesity and healthy controls. These trajectories, coupled with the standard deviation bars, facilitated the rigorous tracking and assessment of gait changes for each participant throughout the 6-week study period.

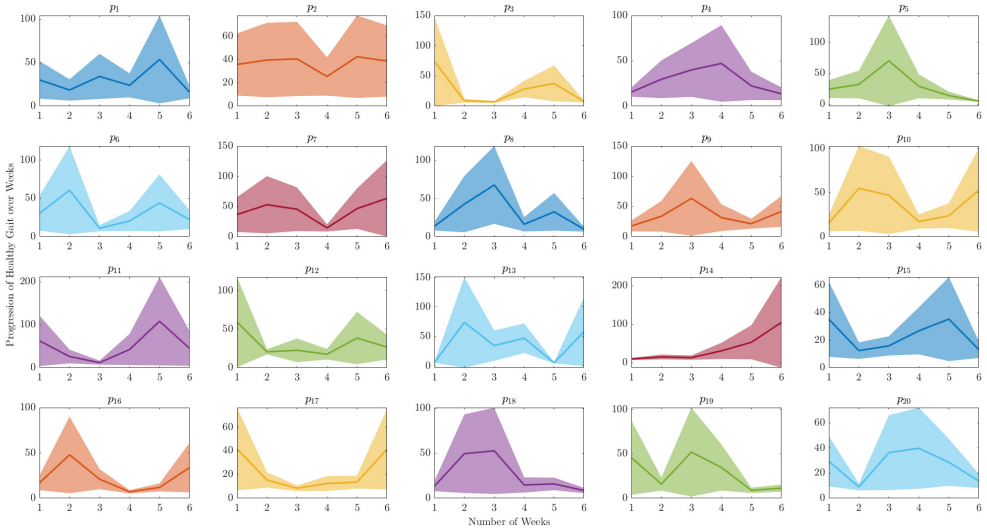

Figure 8. The advancement of normal walking patterns for each person over a 6-week period is shown.

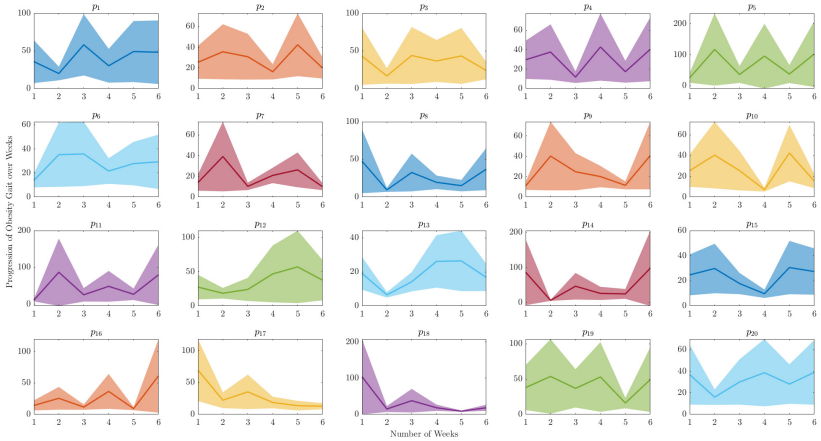

Figure 9. Tracking the improvement in gait for managing obesity for each person over a 6-week period is shown.

4. Experiment Results

In this section, we present the findings of our experimental investigation, which encompasses the performance of the SVM classifier in identifying gait patterns for both

healthy control and obese groups. Additionally, we examine the impact of various Kernel SVM model parameters on classification performance. A comprehensive analysis of the generalisation performance of the SVM classifier is also presented, including the Receiver Operating Characteristic (ROC) curve, the area under the ROC curve, and the SVM decision classification boundary. The results demonstrate the potential of using SVM in combination with a controlled CA model for accurate detection of gait patterns associated with healthy controls and individuals with obesity.

4.1. Receiver Operating Characteristic (ROC) Curve

The Receiver Operating Characteristic (ROC) curve is a graphical representation of the performance of a binary classifier system as the discrimination threshold is varied [19]. In the context of SVM, the ROC curve is used to evaluate the performance of the SVM classifier in classifying data samples into two different classes. The ROC curve plots the true positive rate (TPR) (sensitivity) against the false positive rate (FPR) ($\approx 1 - \text{TNR}$) at various threshold settings. Figures 10–12 illustrate the ROC curves for the best pair of σ and C values that satisfy the highest accuracy during the entire trial period.

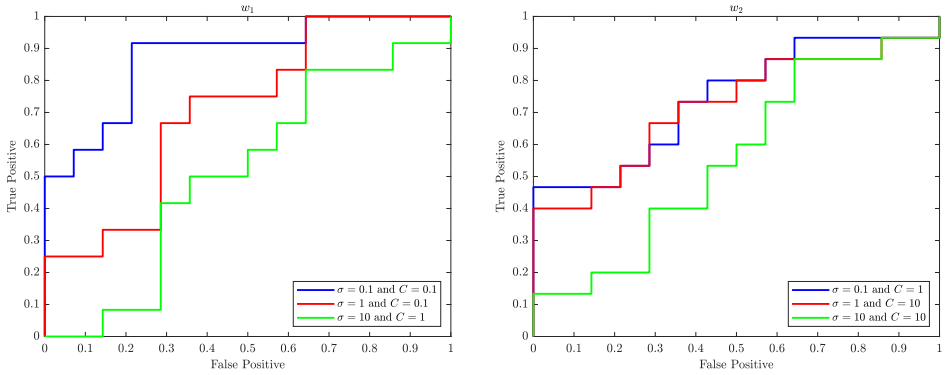

Figure 10. The relationship between True Positive Rate (Sensitivity) and False Positive Rate (1-Specificity) at various threshold levels, as determined by the kernel function of the SVM, is displayed through the ROC curves of w_1 and w_2.

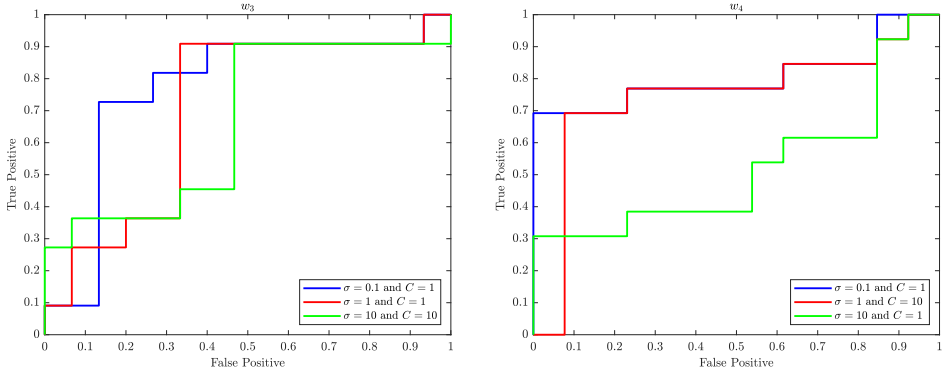

Figure 11. The relationship between True Positive Rate (Sensitivity) and False Positive Rate (1-Specificity) at various threshold levels, as determined by the kernel function of the SVM, is displayed through the ROC curves of w_3 and w_4.

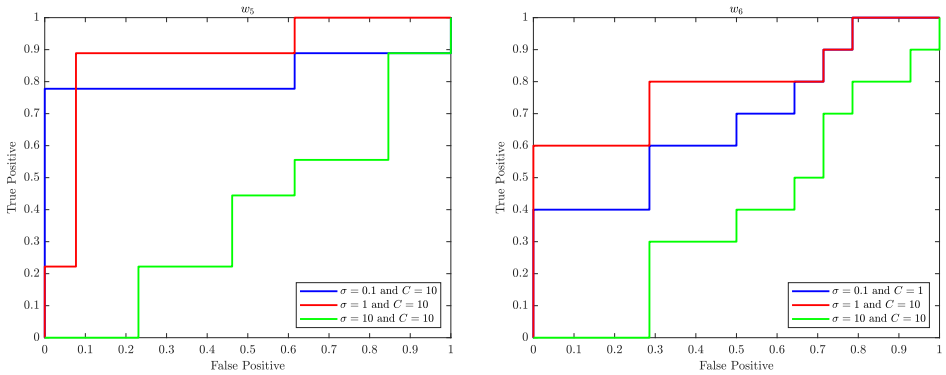

Figure 12. The relationship between True Positive Rate (Sensitivity) and False Positive Rate (1-Specificity) at various threshold levels, as determined by the kernel function of the SVM, is displayed through the ROC curves of w_5 and w_6.

The ROC plots (Figures 10–12) show that, in the context of SVM, parameter C controls the trade-off between maximising the margin and minimising the misclassification error. When the value of C is smaller, such as $C = 0.1$, the margin becomes wider, but there are more instances of misclassifications. Conversely, a larger value of C, such as $C = 10$, leads to a narrower margin, but with a reduced number of misclassifications. Parameter σ is used to control the width of the Kernel Gaussian function that is used to map the input data into a higher-dimensional space, where a linear boundary can be found. A larger value of σ results in a wider Gaussian function, which leads to a softer decision boundary and a higher bias, while a smaller value of σ results in a narrower Gaussian function, which leads to a harder decision boundary and a higher variance.

When σ is small, the decision boundary is more sensitive to input data, which can lead to overfitting. On the other hand, when σ is large, the decision boundary is less sensitive to input data, which can lead to underfitting. Therefore, the value of σ has an impact on generalisation performance of the SVM.

A good value for C and σ is the one that balances the trade-off of bias and variance, that is, a good balance between overfitting and underfitting.

The ROC curves shown in Figures 10–12 perform well with $\sigma = 0.1$ and 1 for various values of C of the SVM, which is likely because the classifier is able to find a good balance between overfitting and underfitting by adjusting the value of C and σ which in turn results in good performance.

4.2. The Area under the Curve (AUC)

The area under the ROC curve is a measure of the performance of a binary classifier [20]. In the context of SVM, the AUC represents the ability of the classifier to distinguish between positive and negative classes. A higher AUC value indicates that the classifier is able to correctly classify more instances of the positive class as positive, while also correctly classifying more instances of the negative class as negative. An AUC of 1.0 represents a perfect classifier, while an AUC of 0.5 represents a classifier that performs no better than random guessing.

Figures 13–15 show how the performance of the SVM model changes as the regularisation parameter strength C is varied. Regularisation parameter C controls the trade-off between maximising the margin (the distance between the decision boundary and the closest training instances) and minimising the classification error. When C is small, the model focuses more on maximising the margin, which can lead to a simpler decision boundary but also a higher classification error. As C is increased, the model focuses more on minimising the classification error, which can lead to a more complex decision boundary but also lower classification error. From Figures 13–15, if the AUC increases as C increases, it means that the model's performance is improving as regularisation strength C increases. This may suggest that the model is underfitting the data when C is small and that increasing the

regularisation strength helps to improve the model's performance. On the other hand, if the AUC decreases as C increases, it means that the model's performance worsens as the regularisation strength increases. This may suggest that the model is overfitting the data when C is small and that increasing regularisation strength C causes the model to become too simplistic and lose important information from the data.

The optimal value of C is where the AUC is the highest; this is the sweet spot where the model is able to balance the trade-off between maximising the margin and minimising the classification error in a way that leads to the best classification performance.

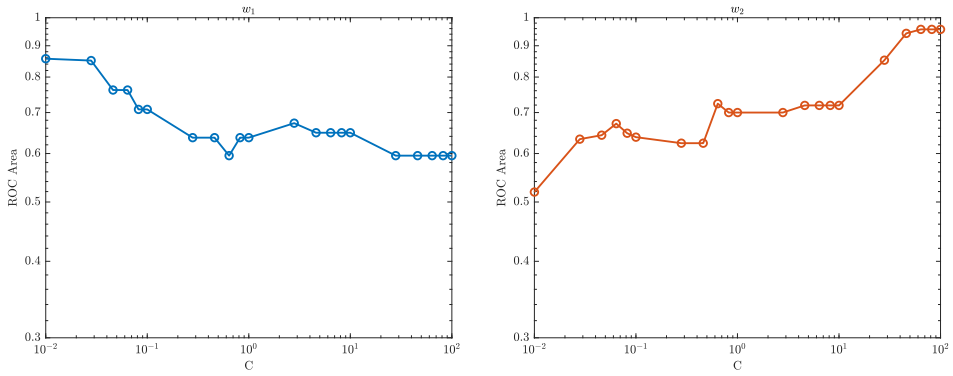

Figure 13. The relationship between the AROC and regularisation parameter C for w_1 and w_2 is presented.

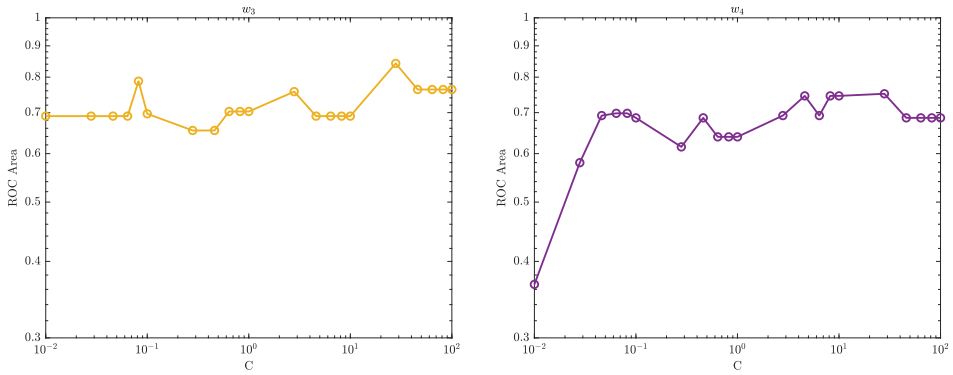

Figure 14. The relationship between the AROC and regularisation parameter C for w_3 and w_4 is presented.

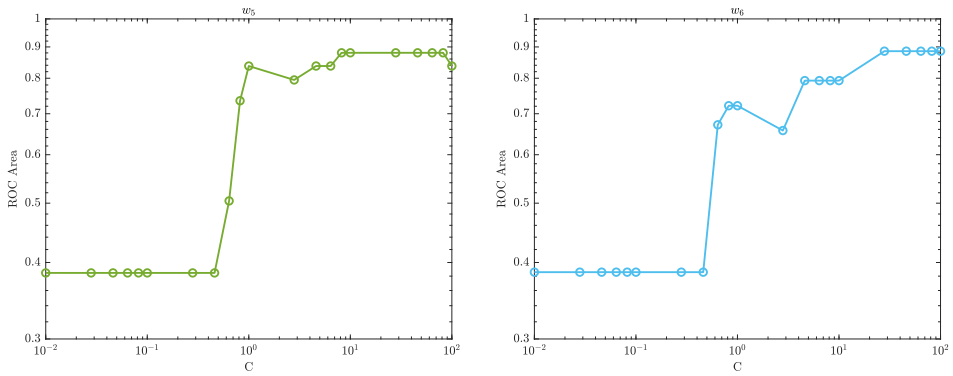

Figure 15. The relationship between the AROC and regularisation parameter C for w_5 and w_6 is presented.

4.3. The Classification Decision Boundary of SVM

The decision boundary of an SVM classifier is determined by the support vectors, which are the data points closest to the boundary. Parameters C and σ, also known as regularisation and kernel parameters, respectively, control the width of the margin and the shape of the decision boundary. For instance, when σ is set to 0.1 and C is set to 1, the decision boundary becomes complex and more influenced by the individual data points. The width of the margin becomes relatively small and the classifier more sensitive to the presence of outliers, as the algorithm tries to minimise misclassification errors. Moreover, when σ is set to 0.1 and C is set to 10, the decision boundary is even more complex as C has a greater influence on the decision boundary. The width of the margin is even smaller and the classifier is even more sensitive to outliers. Furthermore, when σ is set to 0.1 and C is set to 0.1, the decision boundary is relatively simple as C has a much smaller influence on the decision boundary. The width of the margin is relatively large and the classifier is less sensitive to outliers.

The classification boundaries of the SVM model are depicted in Figures 16–18 using the best classification parameters, enabling the model to accurately categorise participants into the appropriate group.

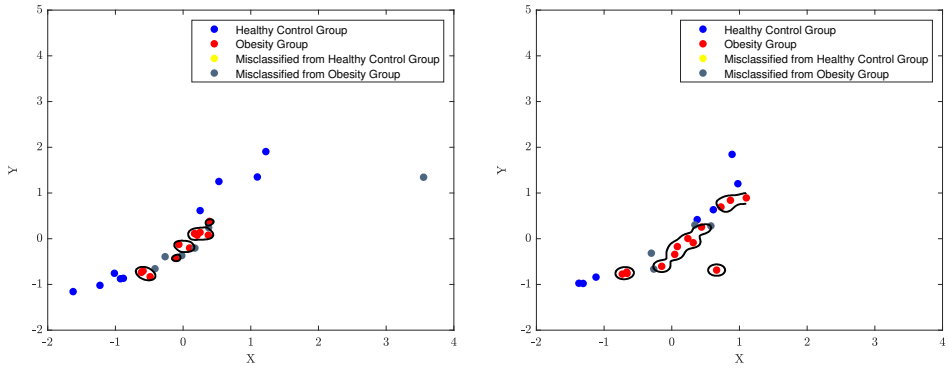

Figure 16. The boundary that separates the healthy control walk patterns from the obesity patterns in an SVM model, with RCC control parameters $f_p = 1$, $f_g = 1$, $x_p = -1$, $x_g = -1$, $\mu_f = 2$, and $\sigma = 0.1$ and $C = 0.1$ for w_1 and $\sigma = 0.1$ and $C = 1$ for w_2, is shown.

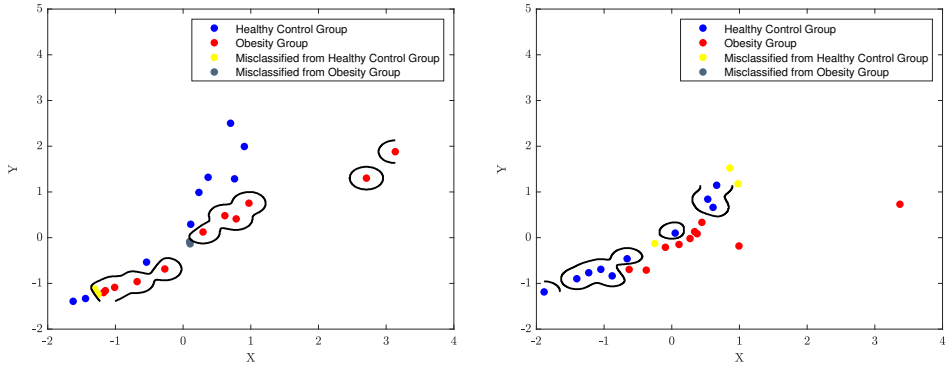

Figure 17. The boundary that separates the healthy control walk patterns from the obesity patterns in an SVM model, with RCC control parameters $f_p = 1$, $f_g = 1$, $x_p = -1$, $x_g = -1$, $\mu_f = 2$, and $\sigma = 0.1$ and $C = 1$ for w_3 and w_4, is shown.

The overall performance of the proposed SVM model is evaluated in Figure 19, where the best classification parameters ($\sigma = 0.1$ and $C = 0.1$) result in the optimal generalisation performance. The 6-week evaluation of the SVM shows fluctuating accuracy in classifying participants into the healthy control and obesity groups. A high accuracy reflects consistent participant characteristics, facilitating accurate classification by the SVM, whereas a low accuracy indicates high variability in participant characteristics, making classification

challenging. In individuals with obesity, the influence of various factors, including walk speed, affects the results depicted in Figure 19. The figure demonstrates that the highest accuracy is observed during the initial week, but experiences a significant decline in the third week. Subsequently, there is a slight improvement in the fourth week, followed by further declines in the fifth and sixth weeks. The fluctuation in the accuracy of the SVM model during the 6-week period, despite the uniform diet and exercise regimen followed by the participants, could be attributed to various reasons such as variations in compliance levels, where some participants may have been more diligent in adhering to the regimen than others, leading to different classifications into healthy control or obesity groups. Other factors include individual differences such as genetics, medical history, and personal habits, measurement inaccuracies, and changes in any of the systems (metabolic, neuromuscular, cardiovascular) altering participant characteristics over time, even when following the prescribed diet and exercise regimen. Participants' stress levels or health status could impact their classification as it could alter variables affecting their gait and hence classification into healthy control or obesity groups.

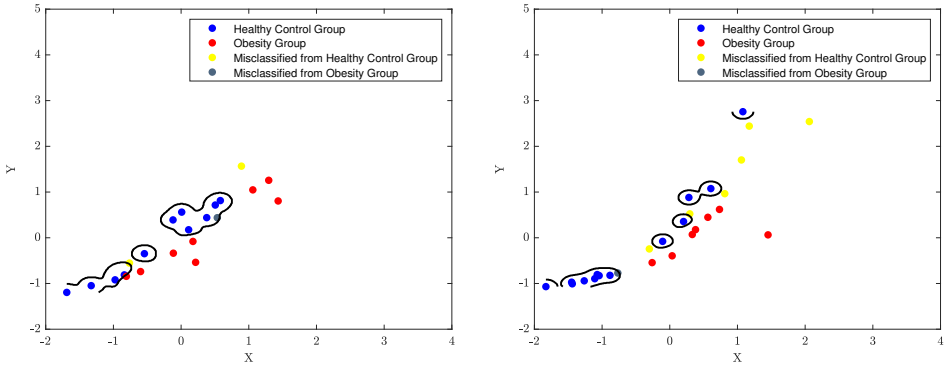

Figure 18. The SVM decision boundary that separates the healthy control walk patterns from the obesity patterns in an SVM model, with RCC control parameters $f_p = 1$, $f_g = 1$, $x_p = -1$, $x_g = -1$, $\mu_f = 2$, and $\sigma = 0.1$ and $C = 10$ for w_5 and $\sigma = 0.1$ and $C = 1$ for w_6, is shown.

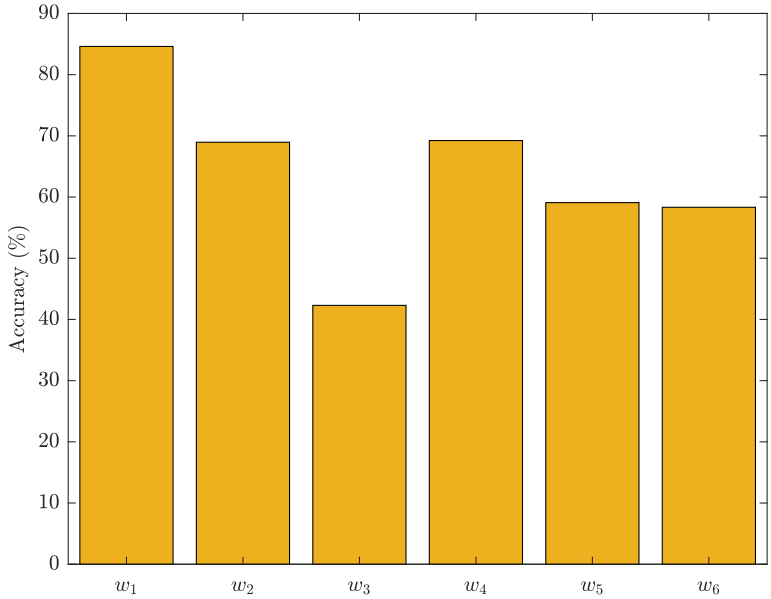

Figure 19. The classification performance of SVM over a 6-week (w_1–w_6) period is presented.

5. Discussion

The primary aim of the comprehensive study was to assess the effectiveness of obesity treatment interventions through the application of a unique CA approach. Simultaneously,

the investigation delved into the intricate dynamics of gait patterns, particularly within the context of obesity. This multifaceted exploration sought to provide a deeper understanding of gait patterns and evaluate the potential of the CA methodology combined with SVM classification in gait analysis within the context of obesity treatment assessment. This multidimensional exploration sought to not only quantify gait variability, but also ascertain the robustness of our CA-SVM methodology for gait classification. Throughout the 6-week study period, SVM classification accuracy exhibited significant fluctuations, with the highest accuracy recorded in the initial week, followed by substantial declines in Weeks 3 through 6. These fluctuations highlight the dynamic nature of SVM model's ability to categorise gait patterns over time. Notably, these variations are not arbitrary but reflect shifts in participant characteristics that significantly impact classification outcomes.

All participants adhered to a uniform diet and exercise regimen during the study, making it evident that individual factors beyond the protocol influenced gait patterns and SVM classifications each week. Factors such as compliance, genetics, medical history, stress levels, or changes in metabolic/neuromuscular systems likely played a role. The SVM accuracy metric robustly quantifies the influence of these individual characteristics on classification performance. ROC curves and AUC values provide insights into the model's proficiency in distinguishing between healthy and obese gait patterns. Optimal model performance occurred under specific parameter settings, $\sigma = 0.1$ and $C = 1$ or 10, where AUC values were maximised. These results confirm the exceptional generalisation capabilities of the SVM model when applied to unseen data and underscore the effectiveness of our CA-SVM methodology in extracting relevant features from gait data.

Visual representations, in the form of phase plots, vividly illustrate the distinctions between healthy and obese gait patterns achieved through the CA method. The phase plots reveal that obese gait patterns are characterised by slower and more labored movements, while healthy gait patterns are smoother and more fluid. These differences align with expectations, given the increased joint stress and stiffness associated with obesity. Phase plots affirm that CA effectively distinguishes between the two groups by revealing interpretable spatio-temporal gait characteristics.

The spatio-temporal analysis quantifying variability in gait progression over a 6-week period offers valuable insights. Notably, wider variability is observed among obese participants compared to their healthy counterparts. This underscores CA's capacity to elucidate subtle yet evolving patterns through phase plot analysis and its competence in quantifying gait variability. Lastly, classification accuracy results, ranging from 78.2% to 90%, strongly validate the efficacy of the CA method in dimensionality reduction and data representation, enhancing classification performance. CA successfully transforms complex gait patterns into lower-dimensional trajectories discernible by the SVM algorithm, leading to high accuracy. This demonstrates CA's proficiency in extracting essential features and capturing nonlinear relationships, enabling precise classification and establishing it as an effective data representation strategy.

6. Conclusions

The Criticality Analysis method for nonlinear data representation can be effectively used to represent gait data and highlight medical conditions. The variability and detection of changes over time highlight the ability of the method to determine changes in gait in response to clinical intervention. The potential to assess clinical disorders using only gait is an exciting development especially for long-term or complex disorders associated with metabolic stress. The combination of nonlinear data representation with supervised machine learning methods can significantly improve the assessment of a patient's status and improve the likelihood of positive outcomes by enabling objective assessment during treatment.

Author Contributions: Conceptualisation, S.E.; methodology, S.E. and T.V.o.S.; validation, S.E.; formal analysis, S.E.; investigation, S.E.; data curation, H.D., J.C., A.A., C.M., M.M.-B., S.L., S.V.-C., M.J.A. and D.F.; writing—original draft preparation, S.E.; writing—review and editing, S.E. and T.V.o.S.; visualisation, S.E.; supervision, T.V.o.S. All authors have read and agreed to the published version of the manuscript.

Funding: This work was supported by a Newton Fund Institutional Links grant (grant ID: 432368181) under the Newton–Mosharafa Fund partnership between the United Kingdom and Mexico. The grant was funded by the UK Department for Business, Energy and Industrial Strategy (BEIS) and delivered by the British Council. The funding supported collaboration activities between Oxford Brookes University and Hospital Infantil de Mexico Federico Gomez under the Newton Institutional Links program administered by the British Council.

Institutional Review Board Statement: Not applicable.

Informed Consent Statement: Not applicable.

Data Availability Statement: In accordance with the General Data Protection Regulation (GDPR) guidelines, the database utilised in this study is maintained in a confidential and secure manner within the purview of the Faculty of Health and Life Sciences at Oxford Brookes University. Owing to privacy considerations, access to the dataset is restricted to authorised personnel only.

Acknowledgments: The authors gratefully acknowledge the support provided by the British Council under the Newton Fund Institutional Links program for making this collaboration possible. We also acknowledge our institutional partners Oxford Brookes University and Hospital Infantil de Mexico Federico Gomez for their support and contribution.

Conflicts of Interest: The authors declare no conflict of interest.

References

1. Kuo, A.D.; Donelan, J.M. Dynamic principles of gait and their clinical implications. *Phys Ther.* **2010**, *90*, 157–174. [CrossRef] [PubMed]
2. Clark, J.E.; Phillips, S.J. A longitudinal study of intralimb coordination in the first year of independent walking: A dynamical systems analysis. *Child Dev.* **1993**, *64*, 1143–1157. [CrossRef] [PubMed]
3. Dingwell, J.B.; Cusumano, J.P. Nonlinear time series analysis of normal and pathological human walking. *Chaos* **2000**, *10*, 848–863. [CrossRef] [PubMed]
4. Glazier, D.S. Metabolic Scaling in Complex Living Systems. *Systems* **2014**, *2*, 451–540. [CrossRef]
5. Hausdorff, J.M.; Mitchell, S.L.; Firtion, R.; Peng, C.K.; Cudkowicz, M.E.; Wei, J.Y.; Goldberger, A.L. Altered fractal dynamics of gait: Reduced stride-interval correlations with aging and Huntington's disease. *J. Appl. Physiol.* **1997**, *82*, 262–269. [CrossRef] [PubMed]
6. Alam, U.; Riley, D.R.; Jugdey, R.S.; Azmi, S.; Rajbhandari, S.; D'Août, K.; Malik, R.A. Diabetic Neuropathy and Gait: A Review. *Diabetes Ther.* **2017**, *8*, 1253–1264. [CrossRef] [PubMed]
7. Toro, B.; Nester, C.; Farren, P. A review of observational gait assessment in clinical practice. *Physiother. Theory Pract.* **2003**, *19*, 137–149. [CrossRef]
8. Pirker, W.; Katzenschlager, R. Gait disorders in adults and the elderly: A clinical guide. *Wien. Klin. Wochenschr.* **2017**, *129*, 81–95. [CrossRef]
9. Sipari, D.; Chaparro-Rico, B.D.M.; Cafolla, D. SANE (Easy Gait Analysis System): Towards an AI-Assisted Automatic Gait-Analysis. *Int. J. Environ. Res. Public Health* **2022**, *19*, 10032. [CrossRef]
10. Guo, Q.; Jiang, D. Method for Walking Gait Identification in a Lower Extremity Exoskeleton Based on C4.5 Decision Tree Algorithm. *Int. J. Adv. Robot. Syst.* **2015**, *12*, 30.
11. Harris, E.J.; Khoo, I.-H.; Demircan, E. A Survey of Human Gait-Based Artificial Intelligence Applications. *Front. Robot. AI* **2022**, *8*, 749274. [CrossRef] [PubMed]
12. McGrath, M.; Howard, D.; Baker, R. The strengths and weaknesses of inverted pendulum models of human walking. *Gait Posture* **2015**, *41*, 389–394. [CrossRef] [PubMed]
13. Berry, H. Chaos in a Bienzymatic Cyclic Model with Two Autocatalytic Loops. *Chaos Solitons Fractals* **2003**, *18*, 1001–1014. [CrossRef]
14. Eltanani, S.; olde Scheper, T.V.; Dawes, H. A Novel Criticality Analysis Technique for Detecting Dynamic Disturbances in Human Gait. *Computers* **2022**, *11*, 120. [CrossRef]
15. olde Scheper, T.V. Criticality Analysis: Bio-inspired Nonlinear Data Representation. *arXiv* **2023**, arXiv:2305.14361.
16. Rota, V.; Perucca, L.; Simone, A.; Tesio, L. Walk ratio (step length/cadence) as a summary index of neuromotor control of gait: Application to multiple sclerosis. *Int. J. Rehabil. Res.* **2011**, *34*, 265–269. [CrossRef] [PubMed]

17. Mobbs, R.J.; Perring, J.; Raj, S.M.; Maharaj, M.; Yoong, N.K.M.; Sy, L.W.; Fonseka, R.D.; Natarajan, P.; Choy, W.J. Gait metrics analysis utilizing single-point inertial measurement units: A systematic review. *Mhealth* **2022**, *8*, 9. [CrossRef] [PubMed]
18. Esser, P.; Dawes, H.; Collett, J.; Howells, K. Insights into Gait Disorders: Walking Variability Using Phase Plot Analysis, Parkinson's Disease. *Gait Posture* **2013**, *38*, 648–652. [CrossRef]
19. Nahm, F.S. Receiver operating characteristic curve: Overview and practical use for clinicians. *Korean J. Anesthesiol.* **2022**, *75*, 25–36. [CrossRef]
20. Bradley, A.P. The use of the area under the ROC curve in the evaluation of machine learning algorithms. *Pattern Recognit.* **1997**, *30*, 1145–1159. [CrossRef]